Chinese Journal of Aeronautics, (2013),26(5): 1147–1155

Chinese Society of Aeronautics and Astronautics
& Beihang University

Chinese Journal of Aeronautics

cja@buaa.edu.cn
www.sciencedirect.com

Active generalized predictive control of turbine tip clearance for aero-engines

Peng Kai [a], Fan Ding [a,*], Yang Fan [a,b], Fu Qiang [a,c], Li Yong [a]

[a] *School of Power and Energy, Northwestern Polytechnical University, Xi'an 710072, China*
[b] *Aeronautics and Astronautics Engineering College, Air Force Engineering University, Xi'an 710038, China*
[c] *School of Flight Technology, Civil Aviation Flight University of China, Guanghan 618307, China*

Received 30 July 2012; revised 16 December 2012; accepted 3 February 2013
Available online 1 August 2013

KEYWORDS

Active clearance control (ACC);
Aero-engine;
Aircraft;
Generalized predictive control (GPC);
Global convergence;
Robust perturbation radius;
Turbine tip clearance

Abstract Active control of turbine blade tip clearance continues to be a concern in design and control of gas turbines. Ever increasing demands for improved efficiency and higher operating temperatures require more stringent tolerances on turbine tip clearance. In this paper, a turbine tip clearance control apparatus and a model of turbine tip clearance are proposed; an implicit active generalized predictive control (GPC), with auto-regressive (AR) error modification and fuzzy adjustment on control horizon, is presented, as well as a quantitative analysis method of robust perturbation radius of the system. The active clearance control (ACC) of aero-engine turbine tip clearance is evaluated in a lapse-rate take-off transient, along with the comparative and quantitative analysis of the stability and robustness of the active tip clearance control system. The results show that the resultant active tip clearance control system with the improved GPC has favorable steady-state and dynamic performance and benefits of increased efficiency, reduced specific fuel consumption, and additional service life.

1. Introduction

The classical modeling and design techniques for engine modeling and control law have been used by the engine control community to solve traditional control problems. Nontraditional control problems, such as multivariable controls, active controls, and life-extending controls, have been studied in recent years. These problems can be grouped in a category called advanced controls (as opposed to the traditional set-point and transient controls). The field of advanced controls is largely in the research stage.[1]

Turbine blade tip clearance continues to be a concern in design and control of gas turbines. A successfully implemented active tip clearance control is expected to have benefits of increased efficiency, reduced specific fuel consumption, and additional service life.[2–4]

Active clearance control (ACC) of the high-pressure turbine (HPT) is one of the techniques that designers use to increase performance of their engines. In most of the new large commercial engines, the size of the turbine case is controlled through cooling

* Corresponding author. Tel.: +86 29 88460221.
E-mail addresses: 330993652@qq.com (K. Peng), fanding@nwpu.edu.cn (D. Fan), bobopro@163.com (F. Yang), fqa311f@163.com (Q. Fu), 46326998@qq.com (Y. Li).

Peer review under responsibility of Editorial Committe of CJA.

ELSEVIER Production and hosting by Elsevier

1000-9361 © 2013 Production and hosting by Elsevier Ltd. on behalf of CSAA & BUAA. Open access under CC BY-NC-ND license.
http://dx.doi.org/10.1016/j.cja.2013.07.005

using compressor bleed air in an open-loop control system. Although open-loop clearance techniques are able to improve performance, many of the engine's actual characteristics responsible for the minimum clearance are unknown. These characteristics include rotor dynamics as well as changes in rotor geometry due to wear or operating condition. Therefore, open-loop techniques must be conservative in closing the gap which results in suboptimal performance. In addition, the use of compressor bleed air results in a system that is unable to rapidly control clearances under more dynamic conditions, such as asymmetric clearance changes during aircraft maneuverings. Clearances reduced within 5–10 mil (1 mil = 0.0254 mm) can improve engine efficiency by several percent points.[5–9] It has been reported by Lattime[3] and Wiseman [5] et al. that, for every 0.001 inch (1 inch = 2.54 cm) decrease in gap in the HPT, specific fuel consumption (SFC) increases 0.1% and engine gas temperature (EGT) increases 1 °C, and noise reduces along with the reduction of aircraft emission, which benefits environment and economy a lot.[10,11]

Increased efficiencies can be achieved by using an active actuation technique that can precisely control clearances at rates sufficient to handle the dynamic conditions encountered during takeoff and landing as well as to provide for optimal clearances during cruise.

2. Model development and active generalized predictive control

The block diagram in Fig. 1 shows the control loop architecture used for clearance control in this paper, which is composed of an aircraft, an aero-engine, a turbine tip clearance apparatus, and control parts. In this section, a nonlinear dynamical model of turbine tip clearance and certain aircraft and aero-engine will be presented, as well as a turbine tip clearance apparatus and an implicit active generalized predictive control (GPC) with auto-regressive (AR) error modification and fuzzy adjustment on control horizon. The active control system for aero-engine turbine tip clearance will be evaluated in a lapse-rate take-off transient.

2.1. The aircraft model

In order to get the inlet condition (the altitude H and the Mach number Ma) of the engine during aircraft maneuverings, the equations of motion for the aircraft are needed (see Fig. 1). The aircraft model can be derived by using the Euler angle approach for an orientation model,[12] but the disadvantage is that the differential equations of motion become singular when the pitch angle θ passes through $\pm\pi/2$. To avoid these singularities and ill-conditioned differential equations, quaternions are used in the aircraft orientation presentation.

Lemma 1. *Let vector* $\boldsymbol{\alpha}$ *rotate around vector* $\boldsymbol{e}_n$ *by angle* γ *and get vector* β*, then*

$$\boldsymbol{\beta} = \boldsymbol{u}\boldsymbol{\alpha}\boldsymbol{u}^{-1} \tag{1}$$

where $\boldsymbol{u}$ *is a quaternion and* $\boldsymbol{u} = \cos\frac{\gamma}{2} + \boldsymbol{e}_n \sin\frac{\gamma}{2}$, $\boldsymbol{u}^{-1} = \cos\frac{\gamma}{2} - \boldsymbol{e}_n \sin\frac{\gamma}{2}$. *The proof of Lemma* 1 *is skipped here.*[13]

With Lemma 1 and relations between the quaternion $q_0 + q_1\mathbf{i} + q_2\mathbf{j} + q_3\mathbf{k}$ and the roll angle ϕ, the pitch angle θ, the yaw angle ψ,[14] we can have an aircraft system representation existing of 13 scalar first-order differential equations:

$$\begin{cases} \dot{u} = rv - qw + \dfrac{1}{m}(\overline{X} + F_{\mathrm{T}}) - 2(q_1q_3 - q_0q_2)g \\ \dot{v} = pw - ru + \dfrac{1}{m}\overline{Y} + 2(q_2q_3 + q_0q_1)g \\ \dot{w} = qu - pv + \dfrac{1}{m}\overline{Z} + (q_0^2 - q_1^2 - q_2^2 + q_3^2)g \end{cases} \tag{2}$$

$$\begin{cases} \dot{p} = (c_1r + c_1p)q + c_3\overline{L} + c_4(\overline{N} + h_{\mathrm{E}}q) \\ \dot{q} = c_1pr - c_6(p^2 - r^2) + c_7(\overline{M} + F_{\mathrm{T}}z_{\mathrm{T}} - h_{\mathrm{E}}r) \\ \dot{r} = (c_8p - c_2r)q + c_4\overline{L} + c_9(\overline{N} + h_{\mathrm{E}}q) \end{cases} \tag{3}$$

$$\begin{bmatrix} \dot{q}_0 \\ \dot{q}_1 \\ \dot{q}_2 \\ \dot{q}_3 \end{bmatrix} = \frac{1}{2}\begin{bmatrix} 0 & -p & -q & -r \\ p & 0 & r & -q \\ q & -r & 0 & p \\ r & q & -p & 0 \end{bmatrix}\begin{bmatrix} q_0 \\ q_1 \\ q_2 \\ q_3 \end{bmatrix} \tag{4}$$

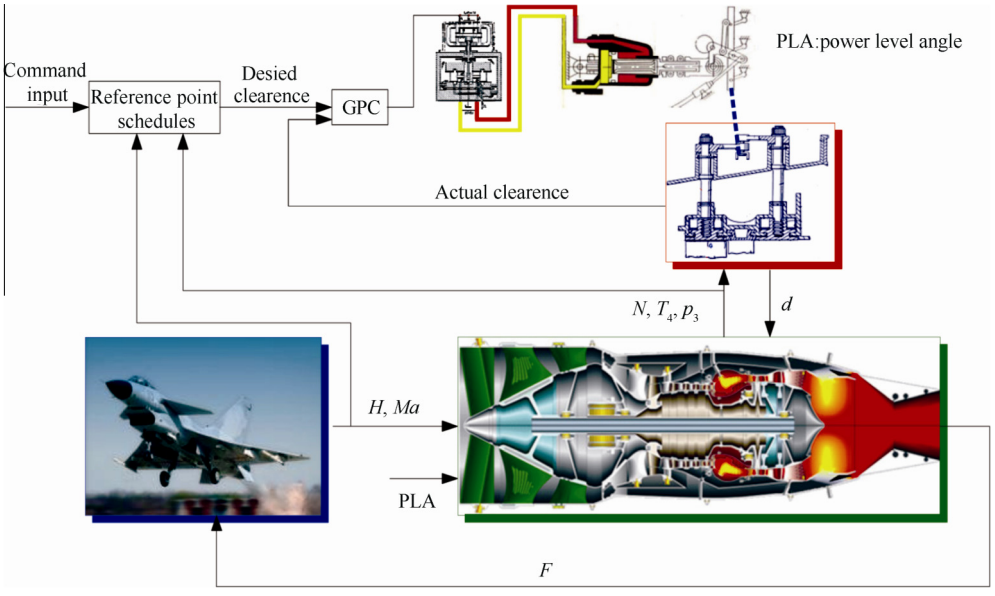

Fig. 1 Block diagram of the whole system for turbine tip clearance control.

$$\begin{bmatrix}\dot{x}_E\\ \dot{y}_E\\ \dot{z}_E\end{bmatrix}=\begin{bmatrix}q_0^2+q_1^2-q_2^2-q_3^2 & 2(q_1q_2-q_0q_3) & 2(q_1q_3+q_0q_2)\\ 2(q_1q_2+q_0q_3) & q_0^2-q_1^2+q_2^2-q_3^2 & 2(q_2q_3-q_0q_1)\\ 2(q_1q_3-q_0q_2) & 2(q_2q_3+q_0q_1) & q_0^2-q_1^2-q_2^2+q_3^2\end{bmatrix}\begin{bmatrix}u\\ v\\ w\end{bmatrix} \tag{5}$$

$$\begin{bmatrix}q_0\\ q_1\\ q_2\\ q_3\end{bmatrix}=\pm\begin{bmatrix}\cos\phi/2\cos\theta/2\cos\psi/2+\sin\phi/2\sin\theta/2\sin\psi/2\\ \sin\phi/2\cos\theta/2\cos\psi/2-\cos\phi/2\sin\theta/2\sin\psi/2\\ \cos\phi/2\sin\theta/2\cos\psi/2+\sin\phi/2\cos\theta/2\sin\psi/2\\ \cos\phi/2\cos\theta/2\sin\psi/2+\sin\phi/2\sin\theta/2\cos\psi/2\end{bmatrix} \tag{6}$$

where m is the mass of the aircraft, g the gravity constant, and z_T is an offset from the center of gravity along the z-axis that the thrust F_T lies in the xOz-plane of the body-fixed reference frame F_B. Expressing the velocity vector $\boldsymbol{V}$ and the total angular velocity $\boldsymbol{\omega}$ of the aircraft with respect to the body-fixed frame F_B gives $\boldsymbol{V}=u\mathbf{i}+v\mathbf{j}+w\mathbf{k}$ and $\boldsymbol{\omega}=p\mathbf{i}+q\mathbf{j}+r\mathbf{k}$. $\overline{X}$, $\overline{Y}$ and $\overline{Z}$ are the components of the aerodynamics force in the frame F_B respectively, while $\overline{L}$, $\overline{M}$ and $\overline{N}$ the components of the aerodynamics moment respectively. The coefficients c_1-c_9 in Eq. (3) are relevant to the moment of inertia of the aircraft in the body-fixed frame. x_E, y_E and z_E are the coordinates of the aircraft in the earth frame. h_E is the engine angular momentum.

From z_E and $\boldsymbol{V}$, the altitude H and the Mach number Ma can be derived.

2.2. The aero-engine model

The model of the aero-engine is described by a set of nonlinear equations, which is a so-called component-based method. Similar to the characteristic of the compressor with stators, the turbine performance map is described by

$$L_T=T\cdot f(n_{T,cor},W_{cor},d) \tag{7}$$

$$\eta_T=g(n_{T,cor},W_{cor},d) \tag{8}$$

where L_T is the turbine power, T the inlet total temperature, $n_{T,cor}$ the corrected speed, W_{cor} the corrected mass flow, d the turbine tip clearance, η_T the turbine adiabatic efficiency; f and g are the functional relationships between above variables.

2.3. The turbine tip clearance apparatus and its model

The efficiency of a gas turbine engine is dependent upon many factors, one of which is the radial clearance between adjacent rotating and non-rotating components, such as the rotor blade tips and the casing shroud surrounding the outer tips of the rotor blades (gap G in Fig. 2). If the clearance is too big, an unacceptable degree of gas leakage will occur with a resultant loss in efficiency. If the clearance is too small, there is a risk that under certain conditions contact will occur between the components.

The potential for contact occurring is particularly acute when the engine's rotational speed is changing, either increasing or decreasing, since temperature differentials across the engine frequently result in the rotating and non-rotating components radially expanding or contracting at different rates. For instance, upon engine accelerations, thermal growth of the rotor typically lags behind that of the casing. During steady-state operations, the growth of the casing ordinarily matches more closely to that of the rotor. Upon engine decelerations, the casing contracts more rapidly than the rotor.

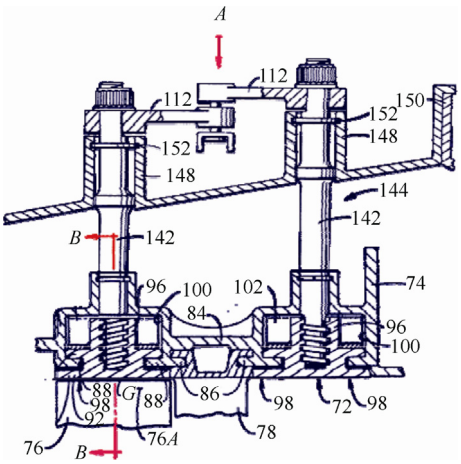

(a) A longitudinal axial sectional view of the clearance control apparatus

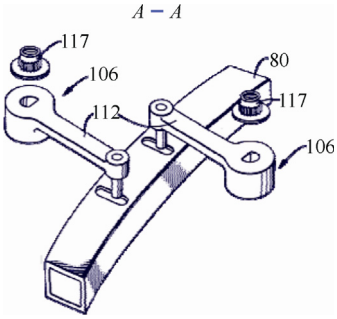

(b) An exploded perspective view of components for actuating the clearance control apparatus

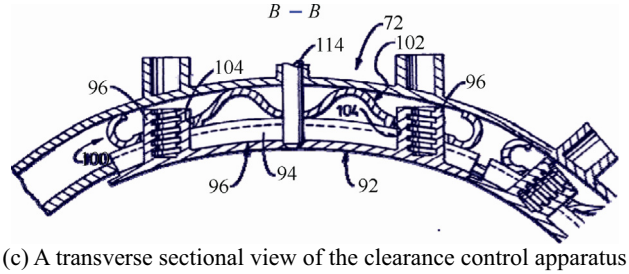

(c) A transverse sectional view of the clearance control apparatus

Fig. 2 A mechanical rotor blade tip clearance control apparatus.

Control mechanisms, usually mechanically or thermally actuated, have been proposed in previous literature to maintain blade tip clearance substantially constant. However, none of them are believed to represent the optimum design for controlling clearance. Consequently, a need still remains for an improved mechanism for clearance control that will permit maintenance of a minimum rotor blade tip-to-shroud clearance throughout the operating range of an engine and thereby improve engine performance and reduce fuel consumption.

A mechanical clearance control apparatus presented herein provides a radial adjustment mechanism for a mechanical rotor blade tip clearance control apparatus in Fig. 2, which satisfies the aforementioned needs and achieves the foregoing objectives.

The clearance control apparatus operable for controlling the clearance employs a radial adjustment mechanism, while the

clearance between the stationary casing 74 and the rotor (not shown) of a gas engine is represented by the outer tips 76*A* of the rotor blades 76 (shown in Fig. 2) which extend radially outwardly in an alternating fashion between the stator vanes 78 which, in turn, are stationarily attached to and extend radially inwardly from the casing 74. The screw 142 is rotatably mounted through the bosses 74 and 148 formed respectively in the inner stationary casing 74 and the outer casing 150. The snap ring 152 on the screw 142 and an annular shoulder (disposed over the snap ring 152) permit the screw 142 to rotate relative to the boss 148, but prevent axial movement thereof. Rotation of the screw 142 relative to the internally threaded bore 96 of the shroud segment 92 therewith results in a radial movement of the shroud segment 92 relative to the rotor without changing the rotational orientation of the screw 142 and its connection to the lever arm 112 connected by the unison ring 80 driven by the hydraulic actuating cylinder.

The biasing means of the clearance control apparatus 72 is preferably the wave spring 102 disposed in the channel 104. The wave spring 102 is in the form of an elongated strip having an undulating configuration along the longitudinal cross section through the strip. The spring 102 has a pair of the spaced openings 104 defined for mounting the spring on the shroud extending through the spring openings 104 so as to prevent movement of the spring 102 longitudinally within the channel 100 relative to the shroud segment 92.

The proposed model of the clearance control apparatus in Fig. 2 incorporates three basic elements – a shroud, a turbine rotor (or disk), and a turbine blade, as shown in Fig. 3. In order to predict deflection of each element due to thermal and mechanical stresses, the temperature, pressure, and force distributions in each element must be modeled. The engine model described in Section 2.2 is employed to provide speed, temperature, and pressure transients for the shroud, rotor, and blade submodels. Each submodel predicts deflections due to thermal and mechanical stresses. As shown in Eq. (9), the relative change in the time-varying geometry of each submodel is then used to calculate the overall change in the clearance d in Eqs. (7) and (8).

$$\begin{aligned} d(t) &= r_{\text{shroud}}(t) - r_{\text{rotor}}(t) - l_{\text{blade}}(t) \\ &= (r_a + u_{s1} + u_{s2}) - (r_0 + u_{s1} + u_{s2}) - (L + u_{s1} + u_{s2}) \end{aligned} \quad (9)$$

where $r_{\text{shroud}}(t)$, $r_{\text{rotor}}(t)$ and $l_{\text{blade}}(t)$ are respectively, the shroud inner radius, the rotor outer radius, and the blade length as a function of time; r_a, r_0 and L are the initial geometric states of the shroud, the rotor, and the blade, respectively, while the subscripted u's denote deformations due to thermal and mechanical stresses. Herein, the derivation of $r_{\text{shroud}}(t)$ will be detailed and those of $r_{\text{rotor}}(t)$ and $l_{\text{blade}}(t)$ will be omitted due to limited space.

The casing grows due to thermal and pressure differentials. As shown in Fig. 3 (In Fig. 3, T and h denote temperature and convection heat transfer coefficient respectively), the inner surface of the shroud at radius r_a is exposed to heated gas at a temperature approximately equal to the turbine inlet temperature T_{turbine}. The outer surface of the shroud at radius r_b is exposed to compressor discharge air. Compressor bleed air is used to purge the space between the shroud and the casing and the pressure p_{purge} is approximately 80% of $p_{\text{compressor}}$. The outer casing wall, r_e, is exposed to bypass airflow. The shroud in the clearance control apparatus can be modeled as a series of arcs rigidly attached to the outer casing, while the casing is modeled as a hoop-like structure and the stress is symmetrical. Because the shroud is attached to the case in the form of a series of arcs, it is assumed that the abradable material layer maintains its approximate thickness even when thermally stressed, so the total deflection of the shroud and the casing due to a thermal differential can be derived from experimentally or numerically determined thermal expansion

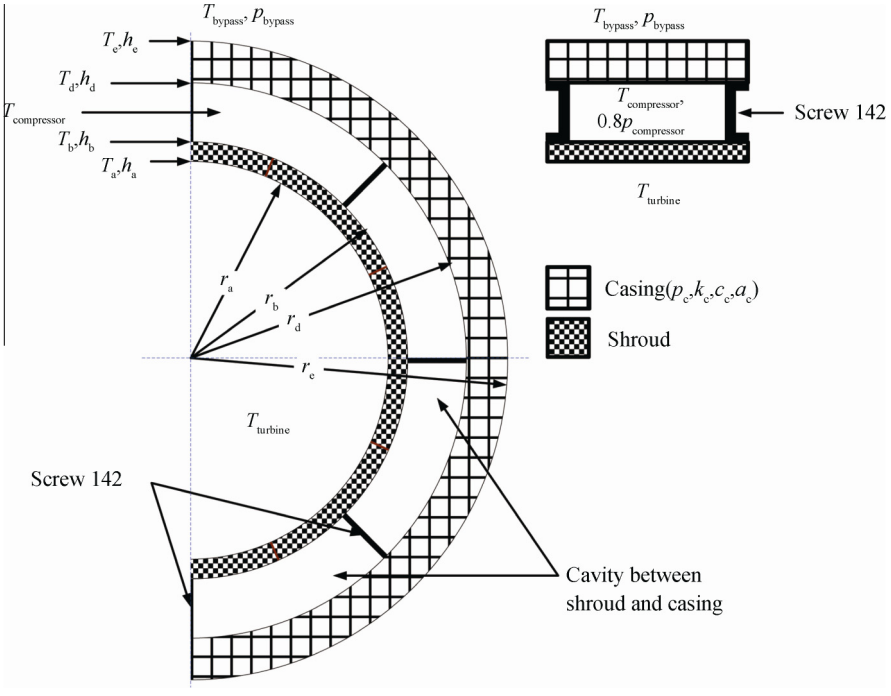

Fig. 3 Schematic of the clearance control apparatus.

coefficient α by using Timoshenko's hollow cylinder equation of thermal stress[15] as shown in Eq. (10).

$$u_{s1} = \alpha r_d \left[T_d + \left(\frac{r_e^2}{r_e^2 - r_d^2} - \frac{1}{2\ln(r_e/r_d)} \right)(T_e - T_d) \right] \tag{10}$$

where r is the radius of the casing wall; subscripts "e" and "d" represent outer and inner. The deflection due to a pressure differential can be derived as follows.

In discussing stresses in a hollow cylinder, etc., it is advantageous to use polar coordinates in which the radial coordinate is often denoted by ρ, and the angular coordinate by φ. If the stress distribution is symmetrical with respect to the axis, the stress components do not depend on φ and are functions of ρ only.[15] The general stress function Φ is

$$\Phi = A\ln\rho + B\rho^2\ln\rho + C\rho^2 + D \tag{11}$$

where A, B, C and D are constants of integration.

In the case of a symmetrical stress distribution,

$$\begin{cases} \sigma_\rho = \dfrac{1}{\rho}\cdot\dfrac{\mathrm{d}\Phi}{\mathrm{d}\rho} \\ \sigma_\varphi = \dfrac{\mathrm{d}^2\Phi}{\mathrm{d}\rho^2} \\ \tau_{\rho\varphi} = \tau_{\varphi\rho} = 0 \end{cases} \tag{12}$$

where σ_ρ, σ_φ, $\tau_{\rho\varphi}$ and $\tau_{\varphi\rho}$ are the normal stress components in the radial and circumferential directions and the shearing-stress components, respectively.

The boundary conditions are:

$$\begin{cases} \sigma_\rho|_{\rho=r_d} = -p_i \\ \sigma_\rho|_{\rho=r_e} = -p_o \end{cases} \tag{13}$$

where p_i is now the mean internal pressure inside the cavity p_{purge}, and p_o is the bypass pressure p_{bypass}.

Substituting Eq. (11) in Eq. (12) and using Eq. (13),

$$\begin{cases} \sigma_\rho = \dfrac{r_d^2 r_e^2(p_o - p_i)}{r_e^2 - r_d^2}\cdot\dfrac{1}{\rho^2} + \dfrac{p_i r_d^2 - p_o r_e^2}{r_e^2 - r_d^2} \\ \sigma_\varphi = -\dfrac{r_d^2 r_e^2(p_o - p_i)}{r_e^2 - r_d^2}\cdot\dfrac{1}{\rho^2} + \dfrac{p_i r_d^2 - p_o r_e^2}{r_e^2 - r_d^2} \end{cases} \tag{14}$$

In the polar coordinate, the strain in the radial direction is

$$\varepsilon_\rho = (\sigma_\rho - \mu\sigma_\varphi)/E \tag{15}$$

where μ is the Poisson's ratio and E is the modulus of elasticity in tension and compression.

Substituting Eq. (14) in Eq. (15) and integrating ε_ρ from 0 to r_d, the deflection due to a pressure differential is obtained:

$$u_{s2} = \frac{1}{E(r_e^2 - r_d^2)}\left[(1-\mu)(p_i r_d^2 - p_o r_e^2) r_d - (1+\mu) r_d r_e^2 (p_o - p_i)\right] \tag{16}$$

2.4. The implicit GPC with AR error modification and fuzzy adjustment on control horizon

Dynamic matrix control (DMC) and generalized predictive control (GPC) are two classes of predictive control systems that have formed applications in many areas. One of the common features of the classical predictive control systems is the direct utilization of plant input and output signals in the closed-loop feedback control, hence avoiding observers in the implementation. There are many modified algorithms of GPC which can be classified as explicit and implicit algorithms. In the explicit GPC, the model parameters of the controlled system are identified firstly, and then Diophantine equations are solved, which involves a large amount of calculation. However, in the implicit GPC, the parameters in the optimal control law are identified by the inputs/outputs of the controlled system, instead of identifying the model parameters of the controlled system, to avoid too much intermediate computation during solving Diophantine equations online.

A novel implicit GPC will be presented next in this paper. The parameters of the optimal control law are identified, based on the farthest-step-ahead prediction and inputs/outputs of the controlled system and the equivalence of GPC and DMC, the prediction error is modified by the AR model of time series of prediction error, and the control horizon is adjusted by means of fuzzy control.

2.4.1. The representation of algorithm structure

Let the prediction model of the controlled system be described by the following matrix polynomial controlled auto-regressive integrated moving average (CARIMA) model[16]:

$$A(z^{-1})y(k) = B(z^{-1})y(k) + C(z^{-1})\xi(k)/\Delta \tag{17}$$

where $A(z^{-1})$, $B(z^{-1})$, $C(z^{-1})$ are polynomials of the backward shift operator z^{-1} with the order n_a, n_b, and n_c, respectively; $y(k)$, $u(k)$, and $\xi(k)$ stand for the output, the control, and the random noise sequence; $\Delta = 1 - z^{-1}$.

The performance index is:

$$J = \sum_{j=1}^{N}[y(k+j) - w(k+j)]^2 + \sum_{j=1}^{N}\lambda(j)[\Delta u(k+j-1)]^2$$

where N is the prediction horizon; $\lambda(j)$ is weighting coefficient of the control increment Δu, and $w(k)$ is the reference trajectory of the output,

$$w(k+j) = \tilde{\alpha}^j y(k) + (1 - \tilde{\alpha}^j) y_r$$

where $\tilde{\alpha}$ is the output softness parameter, $0 < \tilde{\alpha} < 1$, and y_r is the desired output.

The performance index can be rewritten in the vector form as below:

$$J = (\boldsymbol{Y} - \boldsymbol{W})^{\mathrm{T}}(\boldsymbol{Y} - \boldsymbol{W}) + \boldsymbol{\Lambda}\Delta\boldsymbol{U}^{\mathrm{T}}\Delta\boldsymbol{U} \tag{18}$$

where $\boldsymbol{Y} = [y(k+1)\ y(k+2)\cdots y(k+N)]^{\mathrm{T}}$ is the system output; $\boldsymbol{W} = [w(k+1)\ w(k+2)\cdots w(k+N)]^{\mathrm{T}}$ is the reference output; $\boldsymbol{\Lambda} = \mathrm{diag}([\lambda(k+1)\ \lambda(k+2)\cdots\lambda(k+N)])$, and $\Delta\boldsymbol{U} = [\Delta u(k)\ \Delta u(k+1)\cdots\Delta u(k+N-1)]^{\mathrm{T}}$.

Two Diophantine equations are introduced to drive the j-step ahead prediction of the output:

$$T(z^{-1}) = E_j(z^{-1})A(z^{-1})\Delta + z^{-j}F_j(z^{-1}) \tag{19}$$

$$B(z^{-1})E_j(z^{-1}) = G_j(z^{-1})T(z^{-1}) + z^{-j}H_j(z^{-1}) \tag{20}$$

where $T(z^{-1}) = 1 - t_1 z^{-1}$, $0 \leqslant t_1 < 1$ is a filter to weaken the colored noise, $E_j(z^{-1}) = e_{j0} + e_{j1}z^{-1} + \ldots + e_{j,j-1}\ z^{-j+1}$, $F_j(z^{-1}) = f_{j0} + f_{j1}z^{-1} + \ldots + f_{jn}z^{-n}$, $G_j(z^{-1}) = g_0 + g_1 z^{-1} + \ldots + g_{j-1}z^{-j+1}$, $\deg G_j(z^{-1}) = j-1$, and $\deg H_j(z^{-1}) = n_b - 1$.

According to Eqs. (17), (19), and (20), the output $y(k)$ can be given by

$$y(k+j) = G_j(z^{-1})\Delta u(k+j-1) + f(k+j) + \eta(k+j) \tag{21}$$

where

$$f(k+j) = H_j(z^{-1})\Delta u_f(k-1) + F_j(z^{-1})y_f(k),$$
$$u_f(k) = u(k)T^{-1}(z^{-1}),$$
$$y_f(k) = y(k)T^{-1}(z^{-1}),$$
$$\eta(k+j) = E_j(z^{-1})C_j(z^{-1})T^{-1}(z^{-1})\xi(k+j).$$

Eq. (21) can be rewritten in the vector form as:

$$\boldsymbol{Y} = \boldsymbol{G}\Delta\boldsymbol{U} + \boldsymbol{H}\Delta u_f(k-1) + \boldsymbol{F}y_f(k) + \boldsymbol{\eta} = \boldsymbol{G}\Delta\boldsymbol{U} + \boldsymbol{f} + \boldsymbol{\eta} \tag{22}$$

where

$$\boldsymbol{f} = [f(k+1)\ f(k+2)\ \cdots\ f(k+N)]^{\mathrm{T}},$$

$$\boldsymbol{\eta} = [\eta(k+1)\ \eta(k+2)\ \cdots\ \eta(k+N)]^{\mathrm{T}},$$

$$\boldsymbol{H} = [H_1(z^{-1})\ H_2(z^{-1})\ \cdots\ H_N(z^{-1})]^{\mathrm{T}},$$

$$\boldsymbol{F} = [F_1(z^{-1})\ F_2(z^{-1})\ \cdots\ F_N(z^{-1})]^{\mathrm{T}},$$

$$\boldsymbol{G} = \begin{bmatrix} g_0 & 0 & \cdots & 0 \\ g_1 & g_0 & \cdots & 0 \\ \vdots & \vdots & & \vdots \\ g_{N-1} & g_{N-2} & \cdots & g_0 \end{bmatrix}.$$

So, the j-step ahead prediction of the output $y(k)$ is:

$$\hat{y}(k+j) = G_j(z^{-1})\Delta u(k+j-1) + f_j(k+j) \tag{23}$$

The vector form of Eq. (23) is

$$\widehat{\boldsymbol{Y}} = \boldsymbol{G}\Delta\boldsymbol{U} + \boldsymbol{f} \tag{24}$$

The optimal control law can be derived by minimizing J with respect to $\Delta\boldsymbol{U}$. Replacing $\boldsymbol{Y}$ in J with $\widehat{\boldsymbol{Y}}$ and letting

$$\frac{\mathrm{d}J}{\mathrm{d}\Delta\boldsymbol{U}} = 0$$

then the optimal control law is consequently

$$\Delta\boldsymbol{U} = [\boldsymbol{G}^{\mathrm{T}}\boldsymbol{G} + \boldsymbol{\Lambda}]^{-1}\boldsymbol{G}^{\mathrm{T}}(\boldsymbol{W} - \boldsymbol{f}) \tag{25}$$

(1) Identification of parameters $\boldsymbol{G}$ and $\boldsymbol{f}$ in the optimal control law

From Eqs. (19) and (20),

$$G_j(z^{-1}) = [B(z^{-1})E_j(z^{-1}) - z^{-j}H_j(z^{-1})]T^{-1}(z^{-1})$$
$$= \frac{B(z^{-1})}{A(z^{-1})\Delta}[1 - z^{-j}F_j(z^{-1})T^{-1}(z^{-1})] - z^{-j}H_j(z^{-1})T^{-1}(z^{-1})$$

then $\boldsymbol{G}_j(z^{-1})$ is the first j terms of the step response of the controlled system

$$G_j(z^{-1}) = g_0 + g_1 z^{-1} + \ldots + g_{j-1}z^{-j+1}$$

So the matrix $\boldsymbol{G}$ in GPC is equal to the system matrix in prediction equations of DMC, and the expression of the optimal control law Eq. (25) is also consistent with that of DMC, while the optimal control solution is unique to the same linear system under the same objective function. All these mean that $\boldsymbol{f}$ in Eq. (25) is the open-loop prediction of the system output based on the last input/output without the action of the control increment $\Delta u(k)$ at time k compared with the DMC method.

(i) The identification of the matrix $\boldsymbol{G}$

From the Nth equation of the prediction Eq. (22)

$$y(k) = g_{N-1}\Delta u(k-N) + g_{N-2}\Delta u(k-N-1) + \cdots + g_0\Delta u(k-1) + f(k) + \eta(k) \tag{26}$$

All the elements $g_0, g_1, \ldots, g_{N-1}$ in the matrix $\boldsymbol{G}$ appear in Eq. (26), so the identification carried on Eq. (26) can obtain the matrix $\boldsymbol{G}$. Let $\boldsymbol{X}(k) = [\Delta u(k-N)\ \Delta u(k-N+1)\ \cdots u(k-1)\ \ 1]^{\mathrm{T}}$, $\boldsymbol{\theta}(k) = [g_{N-1}\ g_{N-2}\ldots g_0\ \ f(k)]^{\mathrm{T}}$, and then $\boldsymbol{\theta}(k)$ can be updated by using the recursive least squares method with a forgetting factor.

$$\hat{\boldsymbol{\theta}}(k) = \hat{\boldsymbol{\theta}}(k-1) + \boldsymbol{K}(k)(y(k) - \boldsymbol{X}^{\mathrm{T}}(k)\hat{\boldsymbol{\theta}}(k-1))$$
$$\boldsymbol{K}(k) = \boldsymbol{P}(k-1)\boldsymbol{X}(k)(\lambda + \boldsymbol{X}^{\mathrm{T}}(k)\boldsymbol{P}(k-1)\boldsymbol{X}(k))^{-1}$$
$$\boldsymbol{P}(k) = (\boldsymbol{I} - \boldsymbol{K}(k)\boldsymbol{X}^{\mathrm{T}}(k))\boldsymbol{P}(k-1)\lambda^{-1}$$

where λ is the forgetting factor, $0 < \lambda < 1$; $\boldsymbol{K}(k)$ is the gain matrix of innovation, and $\boldsymbol{P}(k)$ is the weighting matrix.

(ii) The identification of the vector $\boldsymbol{f}$

Due to the equivalence of GPC and DMC,

$$\boldsymbol{f} = \begin{bmatrix} f(k+1) \\ f(k+2) \\ \vdots \\ f(k+N) \end{bmatrix} = \begin{bmatrix} g_0 \\ g_1 \\ \vdots \\ g_{N-1} \end{bmatrix}\Delta u(k) + \begin{bmatrix} 1 \\ 1 \\ \vdots \\ 1 \end{bmatrix} e(k),$$

$$e(k) = y(k) - \hat{y}(k).$$

In order to weaken the effect of measurement colored noise on output estimation and accurately estimate vector $\boldsymbol{f}$, an AR error correction method is introduced.

$$\boldsymbol{f} = \begin{bmatrix} f(k+1) \\ f(k+2) \\ \vdots \\ f(k+N) \end{bmatrix} = \begin{bmatrix} g_0 \\ g_1 \\ \vdots \\ g_{N-1} \end{bmatrix}\Delta u(k) + \begin{bmatrix} e(k+1) \\ e(k+2) \\ \vdots \\ e(k+N) \end{bmatrix}$$

where
$e(k+j) = \sum_{i=0}^{N-1} a_i[y(k-i) - \hat{y}(k-i-j)]$, $a_i = \frac{1-b}{1-b^N}b^i$, b is the attenuation coefficient.

(2) Fuzzy adjustment on the control horizon

$\boldsymbol{G}^{\mathrm{T}}\boldsymbol{G} + \boldsymbol{\Lambda}$ is a lower triangular Teoplitz matrix and the matrix inverse $(\boldsymbol{G}^{\mathrm{T}}\boldsymbol{G} + \boldsymbol{\Lambda})^{-1}$ can be calculated by the rapid algorithm. If the control horizon is M, and $\Delta u(k+j) = 0, j > M$, the dimension of $\boldsymbol{G}^{\mathrm{T}}\boldsymbol{G} + \boldsymbol{\Lambda}$ is reduced from N to M. when $M = 1$, the matrix inverse becomes the reciprocal of the scalar. In general, $M = 1$–3, and in order to give attention to both the speed and stability of the system, M can be changed from 3 to 1 smoothly by using fuzzy control. If the diagonal element of $\boldsymbol{G}^{\mathrm{T}}\boldsymbol{G} + \boldsymbol{\Lambda}$ is near to zero, the element $\lambda(i)$ of $\boldsymbol{\Lambda}$ would be increased by the Armijo rule.

2.4.2. The global convergence and robust perturbation radius of the novel implicit GPC

(1) The global convergence

The global convergence of the implicit GPC with AR error modification and fuzzy adjustment of control horizon can be proofed similar to Theorem 11.3.1 in Ref.[17] and it is needless to reiterate here.

(2) The frequency domain analysis of robustness

Considering the additive perturbed model

$$A(G_0(z^{-1}), r(z^{-1})) = \{G_0(z^{-1}) + \Delta_A(z^{-1}) : \|\Delta_A(z^{-1})\| < |r(z^{-1})|, \forall |z| < 1\}$$

where $G_0(z^{-1}) = B(z^{-1})/(A(z^{-1})\Delta)$ is the open-loop transfer function of the nominal system, and the definitions of $A(z^{-1})$ and $B(z^{-1})$ are the same as in Eq. (17).

From Eq. (25), we have

$$\Delta u(k) = [1\ 0\ \cdots\ 0](\boldsymbol{G}^{\mathrm{T}}\boldsymbol{G} + \boldsymbol{\Lambda})^{-1}\boldsymbol{G}^{\mathrm{T}}(\boldsymbol{W} - \boldsymbol{f}) \triangleq \boldsymbol{d}^{T}(\boldsymbol{W} - \boldsymbol{f}) \tag{27}$$

$$\boldsymbol{W} = [\alpha\ \alpha^2\ \cdots\ \alpha^N]^{\mathrm{T}} y(k) + [1-\alpha\ 1-\alpha^2\ \cdots\ 1-\alpha^N]^{\mathrm{T}} y_r \triangleq \boldsymbol{L}y(k) + \boldsymbol{N}y_r \tag{28}$$

$$\boldsymbol{f} = \boldsymbol{H}\boldsymbol{T}^{-1}z^{-1}\Delta u(k) + \boldsymbol{F}\boldsymbol{T}^{-1}y(k) \tag{29}$$

Substituting Eqs. (28) and (29) into Eq. (27) and rearranging,

$$(1 + \boldsymbol{d}^{\mathrm{T}}\boldsymbol{H}\boldsymbol{T}^{-1}z^{-1})\Delta u(k) = \boldsymbol{d}^{\mathrm{T}}\boldsymbol{N}y_r - \boldsymbol{d}^{\mathrm{T}}(\boldsymbol{F}\boldsymbol{T}^{-1} - \boldsymbol{L})y(k) \tag{30}$$

Making the following substitutions: $X = (1 + \boldsymbol{d}^{\mathrm{T}}\boldsymbol{H}\boldsymbol{T}^{-1}z^{-1})$, $Y = \boldsymbol{d}^{\mathrm{T}}\boldsymbol{N}$, $Z = \boldsymbol{d}^{\mathrm{T}}(\boldsymbol{F}\boldsymbol{T}^{-1} - \boldsymbol{L})$, Eq. (30) can be rewritten as

$$Xu(k) = Yy_r - Zy(k) \tag{31}$$

and the close-loop control structure of the system with additive perturbation is shown in Fig. 4.

Let $C = Z/X$ and $D = Y/Z$, and then the closed-loop transfer function of the additive perturbed system is given by the expression

$$G_{\mathrm{pc}} = C(G_0 + \Delta_A)D/[1 + C(G_0 + \Delta_A)] = G_{\mathrm{nc}}(1 + \Delta_A/G_{\mathrm{nc}})D/(1 + \Delta_A G_{\mathrm{nc}}/G_0) \tag{32}$$

where $G_{\mathrm{nc}} = CG_0/(1 + CG_0)$ is the open-loop transfer function of the nominal system.

In order to stabilize the closed-loop perturbed system, the denominator $D^* = 1 + CG_0 + C\Delta_A$ in Eq. (32) is required to satisfy the Nyquist criterion. According to the principle of the small-gain theorem, we have

$$\|\Delta_A\| < \|G_0/G_{\mathrm{nc}}\| = |XA(z^{-1})\Delta + ZB(z^{-1})|/|ZA(z^{-1})\Delta|, \quad \forall |z| \leqslant 1 \tag{33}$$

Theorem 1. *The controller can stabilize the perturbed system set $A(G_0(z^{-1}), r(z^{-1}))$, if the controller $C = Z/X$ sta bilizes the nominal system $G_0(z^{-1}) = B(z^{-1})/[A(z^{-1})\Delta]$, that is, the Shur-stability of the characteristic polynomial $g(z^{-1}) = XA(z^{-1})\Delta + ZB(z^{-1})$ of the nominal system, and the following holds*

$$\|\Delta_A\| < \|G_0/G_{\mathrm{nc}}\| = |XA(z^{-1})\Delta + ZB(z^{-1})|/|ZA(z^{-1})\Delta|, \quad \forall |z| = 1 \tag{34}$$

Proof. Denote $V_1 = \{z : |z| < 1\}$ and $V_2 = \{z : |z| > 1\}$. The zeros of D^* contain all poles of the perturbed system. When the nominal system $g^* = 1 + CG_0$ and the perturbation part $C\Delta_A$ is stable, g^* and $C\Delta_A$ are analytic in the area V_2 and on its boundary $\Gamma = \{z : |z| = 1\} \cup \{z : z \to \infty\}$, so $1 + CG_0(0) > C\Delta_A(0) = 0$,

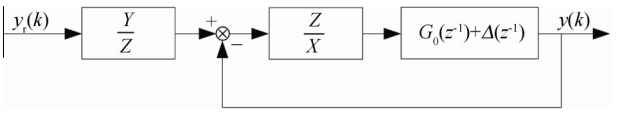

Fig. 4 Schematic for the frequency domain analysis of robustness of the novel implicit GPC.

$z \to \infty |1 + CG_0| > |C\Delta_A|, \forall |z| = 1$ according to condition (34). From the Rouché's theorem,[18] D^* and g^* have the same number of zeros in V_2 and on Γ, so all the zeros of D^* are in V_1, that is, the closed-loop perturbed system and the closed-loop nominal system have consistent stability.

(3) The robust perturbation radius

Let $D^* = d_0 + d_1 z^{-1} + \ldots + d_{n-1}z^{-n+1}$, $g^* = g_0 + g_1 z^{-1} + \ldots + g_{n-1}z^{-n+1}$, and $d_i \in [g_i - \lambda_i R, g_i + \lambda_i R], i = 0,1,\ldots,n-1$, where $\lambda_i > 0$ is the weighting coefficient of the perturbation radius R.

From Theorem 1 and the Rouché's theorem, if $|g^*| > |D^* - g^*|$ holds on $C = \{z : |z| = 1\}$, D^* and g^* have the same number of zeros in V_1, that is, D^* is Shur-stable if g^* is Shur-stable.

Noting that on $C = \{z : |z| = 1\}$, $|D^* - g^*| = \left|\sum_{i=0}^{n-1}(d_i - g_i)z^{-i}\right| \leqslant \sum_{i=0}^{n-1}|d_i - g_i| \leqslant R\sum_{i=0}^{n-1}\lambda_i$.

Thus D^* is Shur-stable if $R < \min_{|z|=1}|g^*|/\sum_{i=0}^{n-1}\lambda_i$, so we take $\min_{|z|=1}|g^*|/\sum_{i=0}^{n-1}\lambda_i$ as an estimation $\widehat{R}$ of the supremum of the robust perturbation radius R. The detail of calculation is presented as below.

On $C = \{z : |z| = 1\}$,

$$|g^*|^2 = g^*(\mathrm{e}^{j\theta})g^*(\mathrm{e}^{j\theta}) = \left[\sum_{i=0}^{n-1} g_i^2\ 2\sum_{i=0}^{n-2} g_i g_{i+1}\ \ldots\ 2\sum_{i=0}^{n-1-k} g_i g_{i+k}\ \ldots\ 2\sum_{i=0}^{n-1-n+1} g_i g_{i+n-1}\right]\boldsymbol{p}$$

where $\boldsymbol{p} = [1\ \cos\theta \cdots \cos(k\theta) \cdots\ \cos[(n-1)\theta]]^{\mathrm{T}}$, $0 \leqslant \theta < 2\pi$.

For $\cos(n\theta)$ belongs to Chebyshev polynomials of the first kind, so

$$\cos(n\theta) = \sum_{k=0}^{\lfloor n/2 \rfloor} C_n^{2k}(\cos^2\theta - 1)^k \cos^{n-2k}\theta$$

$$\boldsymbol{p} = \boldsymbol{T}[1\ \cos\theta\ \cdots\ \cos^{n-1}\theta]^T$$

and when $n = 3$, the coordinate transform matrix $\boldsymbol{T}$ is

$$\boldsymbol{T} = \begin{bmatrix} 1 & 0 & 0 \\ 0 & 1 & 0 \\ -1 & 0 & 2 \end{bmatrix}$$

Thus,

$$|g^*|^2 = \left[\sum_{i=0}^{n-1} g_i^2\ 2\sum_{i=0}^{n-2} g_i g_{i+1}\ \cdots\ 2\sum_{i=0}^{n-1-k} g_i g_{i+k}\ \cdots\ 2\sum_{i=0}^{n-1-n+1} g_i g_{i+n-1}\right] \cdot \boldsymbol{T}[1\ \cos\theta\ \cdots\ \cos^{n-1}\theta]^T \triangleq P(\cos\theta)$$

$$\widehat{R} = \min_{|z|=1}|g^*| \Big/ \sum_{i=0}^{n-1}\lambda_i = \sqrt{\min_{0\leqslant\theta<2\pi} P(\cos\theta)} \Big/ \sum_{i=0}^{n-1}\lambda_i$$

3. Numerical example

In this section, a lapse-rate take-off transient (see Fig. 5) is considered, and the system characteristics and structural parameters of the turbine tip clearance vary largely during the transient. Fig. 6 shows individual deflections and overall clearance with reference to the engine speed transient without clearance adjustment. As expected, the rotor initially responds more quickly due to the centrifugal forces induced by the engine speed transient and the shroud catches up and grows more rapidly due to thermal stresses than either the rotor or the blades, and the pinch point described in Refs.[19,20] can be seen at about 10 s. Turbine clearance (expected to be 30 mil herein), altogether with the fuel flow and the robust perturbation radius, is showed in Fig. 7, respectively, in which Curve 1 is corresponding to the case without clearance adjustment, Curve 2 is under the PID controller with PID parameters optimized by the genetic algorithm, Curve 3 is under the modified LQG controller for fast active turbine tip clearance control systems presented in Refs.[19,20] by NASA Glenn Research Center, and Curve 4 is under the implicit GPC with AR error modification and fuzzy adjustment on control horizon. From Fig. 7(a), the actual clearances under the improved GPC and the modified LQG controller (with slight oscillation) can approach the expected clearance of 30 mil more easily than that under the PID controller (with a certain degree of oscillation); however, the stability and controllability of clearance under the improved GPC is better than those under the PID controller and the modified LQG controller. After the calculations, it shows the fuel flow is reduced by 2% under the PID controller, 4.95% under the modified LQG controller, and 5% under the improved GPC relative to those without clearance active control during the lapse-rate take-off transient, as shown in Fig. 7(b). The robust perturbation radius under the improved GPC is about 0.8% larger than that under the modified LQG controller, 2.1% larger than that under the PID controller, and 3% larger than that without clearance active control, as shown

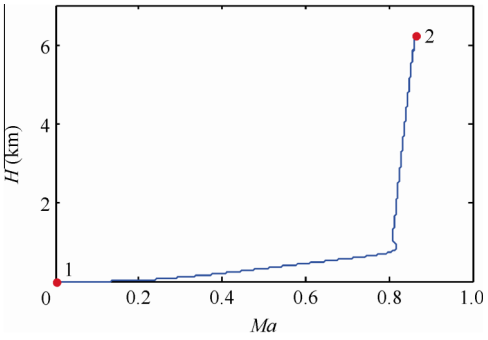

Fig. 5 Flight trajectory of the lapse-rate take-off transient in the flight envelope.

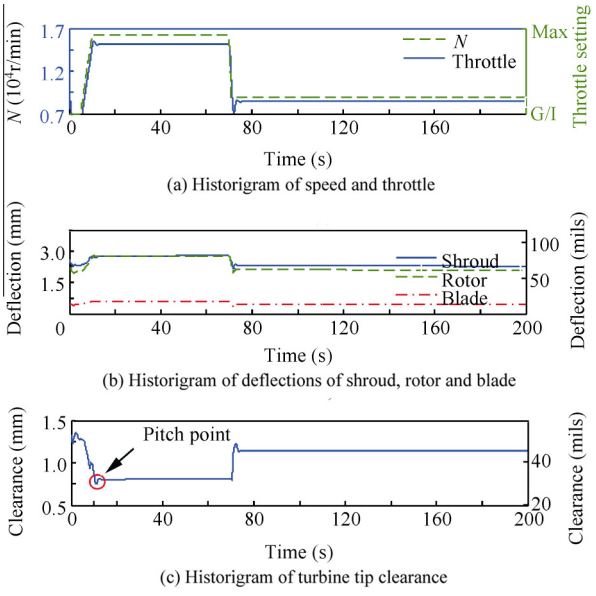

Fig. 6 Deflections and clearance for the lapse-rate take-off transient.

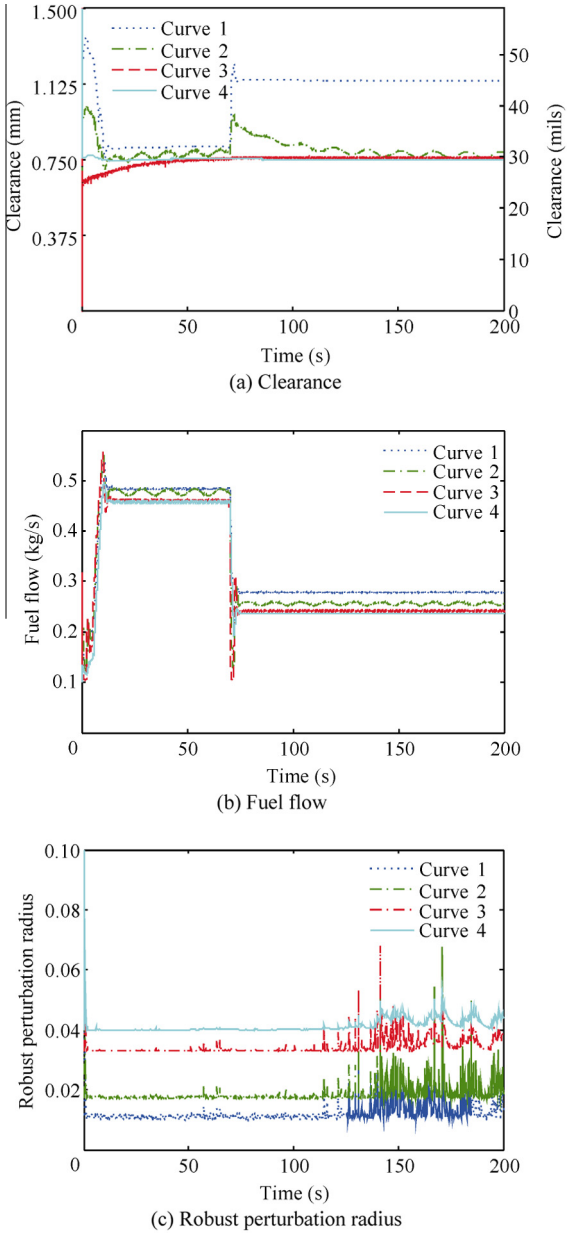

Fig. 7 History chart of some parameters under no control and different controllers.

in Fig. 7 (c), that is, the system stability and robustness under the improved GPC is better than those under the PID controller and the modified LQG controller.

4. Conclusions

(1) In this paper, the active clearance control of turbine tip clearance in a lapse-rate take-off transient is considered and the results show that the stability and controllability of clearance under the improved GPC is better than those under the PID controller and the modified LQG controller presented in some related literature, and furthermore, the fuel flow is smaller and the robust perturbation radius is larger under the improved GPC.

(2) A turbine tip clearance apparatus and an improved GPC can form an active tip clearance system along with other control parts such as actuators, etc. After the comparative analysis, it shows the resultant active tip clearance control system has good static and dynamic performance and benefits of increased efficiency, reduced specific fuel consumption, and additional service life, and it can be used to virtually prototype the controller/actuator mechanism. Future work should involve more detailed research into the active controller and the tip clearance control mechanisms least documented. The current model, controller and the apparatus should also be refined and quantified in order to assess its usefulness for the design of a tip clearance control system used in real engine.

References

1. Jaw LC, Mattingly JD. *Aircraft engine controls: design, system analysis and health monitoring*. New York: American Institute of Aeronautics and Astronautics, Inc; 2009.
2. Ruiz R, Albers B, Sak W, Seitzer K, Steinetz BM. *Benefits of improved HP turbine active clearance control*. NASA/CP-2007-214995/VOL1; 2007.
3. Chupp RE, Hendricks RC, Lattime SB, Steinetz BM, Aksit MF. *Turbomachinery clearance control*. NASA Glenn Research Center, 2007.
4. *Active clearance control system concept performance tests successfully completed at NASA Glenn*. Avaiable from: http://www.grc.nasa.gov/WWW/RT/2005/RX/RX09M-steinetz1.html.
5. Wiseman M W, Guo T. An investigation of life extending control techniques for gas turbine engines. In: *Proceedings of the American control conference*; 2001. p. 3706–7.
6. Peng K, Fan D, Li J, Wu TY. Fuzzy controller design and parameter optimization for aero-engine compressor guide vane system. *J Aerospace Power* 2011;**26**(4):942–6 [Chinese].
7. Jia BH, Zhang XD, Peng K. Dynamic changes rule of aero-engine turbine tip clearance in maneuver flight. *J Aerospace Power* 2011;**26**(12):2757–64 [Chinese].
8. Peng K, Fan D, Bu ZP, Li J, Yin FJ. Failure analysis and parameter optimization for fuel distributor of certain aeroengine. *J Propul Technol* 2011;**32**(2):276–81 [Chinese].
9. Kypuros JA, Melcher KJ. *A reduced model for prediction of thermal and rotational effects on turbine tip clearance*. NASA/TM-2003-212226; 2003.
10. Lattime SB, Steinetz BM. *Turbine engine clearance control systems: current practices and future direction*. NASA/CP-2003-212458/VOL1; 2002.
11. Steinetz BM, Lattime SB, Taylor S, DeCastro JA, Oswald J, Melcher KJ. *Evaluation of an active clearance control system concept*. NASA/TM-2005-213856; 2005.
12. Wu ST, Fei YH. *Flight control system*. Beijing: Beihang University Press; 2009 [Chinese].
13. Liu JF. Three dimensional rotation represented by quaternion. *Coll Phys* 2004;**23**(4):39–43 [Chinese].
14. Xiao YL. *Principle of spacecraft flight dynamics*. Beijing: Aerospace Press; 1995 [Chinese].
15. Timoshenko S, Goodier J. *Theory of elasticity*. New York: McGraw-Hill Book Company; 1970.
16. Camacho EF, Bordons C. *Model predictive control*. London: Springer-Verlag GmbH; 2004.
17. Goodwin GC, Kwai Sang Sin. *Adaptive filtering, prediction and control*. London: Prentice Hall, Inc; 1984.
18. Brown James Ward, Churchill Ruel V. *Complex variables and applications*. 8th ed. New York: McGraw-Hill Book Company; 2009.
19. Garg S. *NASA Glenn research in controls and diagnostics for intelligent aerospace propulsion systems*. NASA/TM-2005-214036; 2005.
20. DeCastro JA, Melcher KJ. A study on the requirements for fast active turbine tip clearance control systems. In: *40th AIAA/ASME/SAE/ASEE joint propulsion conference and exhibit*; 2004 Jul 11–14; Fort Lauderdale, FL; 2004.

Peng Kai is a Ph.D. student in the School of Power and Energy at Northwestern Polytechnical University. His major is aerospace propulsion theory and engineering and current research interests are control systems of aero-engines, etc.

Fan Ding is a professor and Ph.D. advisor in the School of Power and Energy at Northwestern Polytechnical University. His current research interests are design and analysis of control systems of aero-engines, fault diagnosis, engine health management, etc.

Yang Fan is a Ph.D. student in the School of Power and Energy at Northwestern Polytechnical University and a lecturer in the Aeronautics and Astronautics Engineering College at Air Force Engineering University. His current research interests are control systems of aero-engines, etc.

Fu Qiang is a Ph.D. student in the School of Power and Energy at Northwestern Polytechnical University and an associate professor in the School of Flight Technology at Civil Aviation Flight University of China. His current research interest is control systems of aero-engines, etc.

Li Yong is a Ph.D. student in the School of Power and Energy at Northwestern Polytechnical University. His current research interest is control systems of aero-engines, etc.